SCIENCE CHINA
Chemistry

• ARTICLES •

June 2017 Vol.60 No.6: 740–747
doi: 10.1007/s11426-016-9001-5

Controlled fabrication and microwave absorbing mechanism of hollow Fe_3O_4@C microspheres

Yanhui Hou, Huili Yuan, Hang Chen, Junhai Shen & Liangchao Li*

Key Laboratory of the Ministry of Education for Advanced Catalysis Materials, Department of Chemistry, Zhejiang Normal University, Jinhua 321004, China

Received July 30, 2016; accepted January 12, 2017; published online April 26, 2017

Uniform core-shell SiO_2@Fe_3O_4@C microspheres were prepared by a one-step hydrothermal method with SiO_2 microspheres as the template, and the hollow Fe_3O_4@C (HFC) microspheres were achieved via etching SiO_2 template. By changing the sizes of SiO_2 microspheres, a series of HFC microspheres with variable cavity sizes were obtained to study the relationship between cavity size and microwave absorbing (MA) performance for the first time. The morphology and structure of samples were characterized in detail. The results showed that the MA performance of HFC sample depended on its cavity size. In particular, the hollow structure was good for improving MA performance and could make MA move to the high-frequency region. More importantly, as the cavity size increases, the resonance frequency of HFC-*i* (*i*=1,2, 3, 4) samples moved to a low frequency, and the optimal matching thickness of HFC-*i* samples was increasing. Among all HFC-*i* samples, HFC-3 showed the most excellent MA performance, which could be mainly explained by the quarter-wavelength matching model, intrinsical magnetic and dielectric loss. Furthermore, the MA performance of HFC mixture blended by the equal mass fraction of HFC-2, HFC-3 and HFC-4 was the comprehensive results of three HFC-*i* samples. All the above suggested that the cavity size in HFC sample had a great influence on the MA performance.

microwave absorbing, Fe_3O_4@C, cavity size

Citation: Hou Y, Yuan H, Chen H, Shen J, Li L. Controlled fabrication and microwave absorbing mechanism of hollow Fe_3O_4@C microspheres . *Sci China Chem*, 2017, 60: 740–747, doi: 10.1007/s11426-016-9001-5

1 Introduction

In the modern day, environmental pollution has become more and more diversified, not only includes the visible pollution such as air pollution and wastewater [1,2], but also contains the invisible pollution such as omnipresent electromagnetic radiation (EMR) [3,4]. Due to the rapid development of electronic information technology, their negative influence on the environment and human health has become more and more serious. In the scientific community, considerable attention has been paid on the exploration of microwave absorber [5,6]. However, the high-efficiency absorber with the light weight, thin thickness, strong absorption and wide bandwidth is still a challenging task due to the complexity of electromagnetic wave.

In general, there are two common approaches to improve the microwave absorbing (MA) performance of absorber, namely the impedance matching property and attenuation characteristic.

Impedance matching property, i.e., the intrinsic impedance of absorber should be close to that of free space, is an essential prerequisite for the excellent absorber. But in strict sense, the ideal impedance matching property is impossible to come true in the whole frequency range. Encouraging, it could be remedied by regulating the geometrical microstructure of absorber [7]. On the other hand, attenuation characteristic is the final criterion to evaluate MA performance of absorber. It

*Corresponding author (email: sky52@zjnu.cn)

has mentioned that only the absorber with a good impedance matching property can make microwave enter preferably, but if the incident microwave can be not effectively attenuated by absorber, it will pass through absorber. Therefore, an excellent absorber should possess the good attenuation characteristic.

Ferromagnetic materials with the advantageous magnetic loss, as the most traditional absorber, have been reported widely due to the distinguished magnetic performance, such as Fe_3O_4, nickel ferrite, barium ferrite, and manganese ferrite [8–11]. However, the application of ferromagnetic materials has been severely limited owing to its high density and narrow absorbing bandwidth. On the contrary, the carbon materials with the low density and excellent dielectric loss have been investigated in the MA field, including carbon black, carbon fibre, graphene, etc. [12–14]. However, the MA performance of these absorbers, depended only on the single loss mechanism, namely magnetic loss or dielectric loss, can not meet the practical requirement. It has been demonstrated that the excellent MA absorber need a proper impedance matching through the efficient complementarity between complex permeability and permittivity [15]. A lot of researching work has been carried out focusing on above concept, such as $CoFe_2O_4$-graphene, barium ferrite-polypyrrole, and Fe_3O_4-carbon [16–18]. However, the contradictions between impedance matching and attenuation characteristic of materials are difficult to be overcome.

Researchers have attempted to resolve the above contradictions by regulating the structure and morphology of absorber. Among them, the hollow or porous structure shows a huge advantage, because the porous structure is helpful for the penetration of microwave, and the hollow structure can increase the multiple reflection and diffuse scattering of microwave in the inner of absorber [19]. For example, Li *et al*. [20] prepared the hollow Fe_3O_4 nanosphere with the good absorption properties. In addition, many other absorbers, such as the hollow polypryyole, hollow carbon@Fe@Fe_3O_4, hollow graphene-wrapped ZnO [21–23], have been reported and displayed a good MA performance. From the work of Zhang's group [24], the MA performance can be tuned by adjusting the void space of graphene, speculated that the cavity size should have a great influence on MA performance.

In this work, SiO_2@Fe_3O_4@C (SFC) microshperes are successfully prepared by one-step hydrothermal method with SiO_2 as the solid template. After the SiO_2 temple is etched, the hollow Fe_3O_4@C (HFC) microshperes are obtained. The simple synthetic schematic diagram is shown in Figure 1. By changing the sizes of SiO_2 microshperes, a series of hollow Fe_3O_4@C microspheres with variable cavity sizes have been prepared, and the relationship between their cavity size and MA performance is studied for the first time.

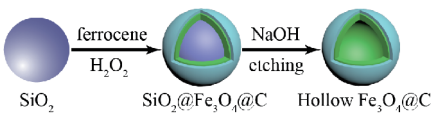

Figure 1 The simple synthetic diagram of HFC microspheres (color online).

2 Results and discussion

2.1 Morphological and structural characterization

The monodispersed SiO_2 nanospheres are shown in Figure 2. It can be seen that the diameter of SiO_2 nanosphere can be controlled by varying tetraethyl silicate (TEOS) concentration, the dosage of solvent (EtOH or 2-propanol (IPA)), H_2O and $NH_3{\cdot}H_2O$. The as-prepared SiO_2 nanospheres possess the smooth surface and good dispersibility, which provide a good platform for loading Fe_3O_4 and carbon. The obtained SFC microspheres presented in Figure S1 (Supporting Information online) still maintain the good dispersity. Compared with SiO_2 nanospheres, the average diameter of corresponding SFC microspheres has increased to some extent, indicating that SiO_2 nanospheres have been coated successfully. More obviously, the surface of SFC microspheres is obvious rougher compared with that of SiO_2 nanospheres. It can be sure that there are many nanoparticles of ~20 nm in the surface of SFC microspheres and some self nucleation Fe_3O_4@C nanoparticles due to the excess ferrocene. The scanning electron microscope (SEM) and transmission electron microscope (TEM) images of HFC microspheres are displayed in Figure 3. It can be found that HFC microspheres keep the good spherical morphology except for very little broken microspheres, while the existence of broken microspheres provides a strong proof for the successful etching of SiO_2 temple and the obtained hollow structure. HFC microspheres present the obvious hollow core-shell structure, and the thickness of carbon shell is about 18 nm. The cavity sizes of HFC-1, HFC-2, HFC-3, and HFC-4 microspheres are 100, 200, 400 and 600 nm respectively.

In order to confirm the phase composition of HFC microspheres further, the X-ray diffraction (XRD) patterns of related samples have been displayed in Figure 4. The broad diffraction peak at 2θ=23° in Figure 4A(a) can be ascribed to the characteristic peak of amorphous SiO_2. However, no characteristic absorption of SiO_2 can be observed in Figure 4A(b–e), suggesting that SiO_2 microshperes have been etched completely. The XRD patterns of all HFC samples present the six clear peaks at 2θ= 30.3°, 35.5°, 43.4°, 53.8°, 57.3° and 62.8°, which are in agreement with (220), (311), (400), (422), (511) and (440) crystal face of spinel-type Fe_3O_4 (JCPDS No. 19-0629). Furthermore, all peaks of HFC microshperes display a little shifting compared

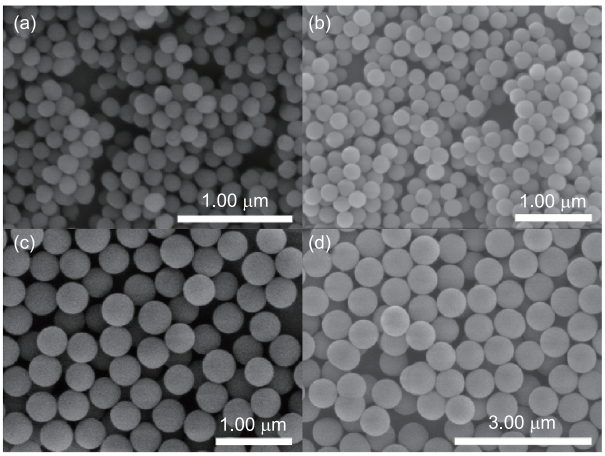

Figure 2 SEM images of SiO_2 microspheres. (a) 100 nm; (b) 200 nm; (c) 400 nm; (d) 600 nm.

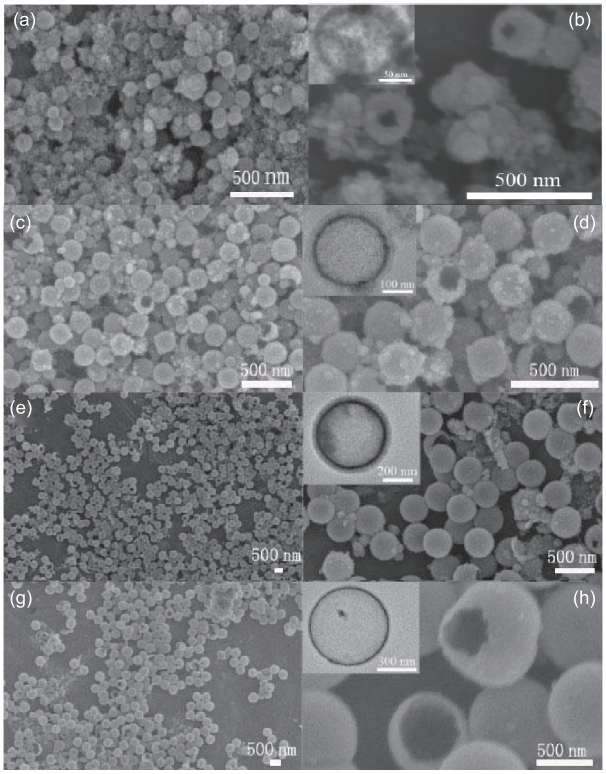

Figure 3 SEM images of HFC microspheres. (a, b) HFC-1; (c, d) HFC-2; (e, f) HFC-3; (g, h) HFC-4. The insets of (b, d, f, h) are the TEM images of HFC microspheres.

with the pure spinel-type Fe_3O_4 [25], indicating the strong interaction between Fe_3O_4 and carbon.

In the preparation of SFC microspheres, the Fe^{2+} in ferrocene can be oxided to Fe_3O_4 under the high temperature, which has been confirmed by above XRD patterns. According to Ref. [26], the cyclopentadienyl in ferrocene can be decomposed into the carbon. Herein, the XPS survey spectrum (Figure 4(B) insert) shows the coexistence of elements

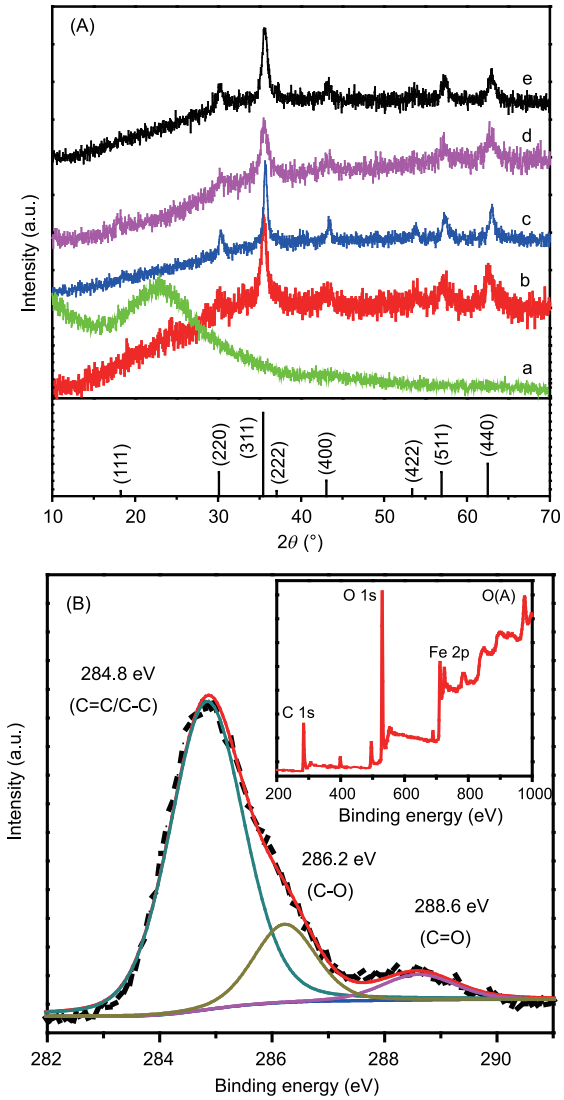

Figure 4 (A) XRD patterns of SiO_2 (a), HFC-1 (b), HFC-2 (c), HFC-3 (d) and HFC-4 (e); (B) C 1s XPS spectra of HFC-3 and the insert is XPS survey of HFC-3 sample (color online).

C, O and Fe in the HFC-3 sample. And the C 1s spectrum includes three main components, namely the C=C/C–C in aromatic rings, C–O of alkoxy and C=O groups [26], suggesting that cyclopentadienyl has been partially oxidized. In addition, the Raman spectrum is used to explore the structure of carbon further. As shown in Figure S2, the Raman peaks of SFC-3 sample located at 1390 and 1598 cm^{-1} are independently assigned to the D and G mode of carbon. And it can be clearly seen that the D peak is broader and weaker than G peak, indicating that the carbon have a tendency of graphitization due to the aromaticity of cyclopentadienyl. So, it can be speculated that the carbon layer in HFC microspheres maybe have the good dielectric loss.

2.2 Magnetic properties

The magnetic hysteresis loops of related samples are shown in

Figure 5, the magnetic parameters including saturation magnetization (M_s) and coercivity (H_c) are listed in Table 1. The M_s values of HFC samples are in the range of 21–23 emu g^{-1} and are less than that of Ref. [26]. It is well known that the M_s value of composite mainly relies on the magnetic component, according to $M_s=\varphi m_s$ (where φ and m_s are the volume fraction and saturation magnetization of magnetic component, respectively [27]), here the m_s of Fe_3O_4 decides the M_s of HFC samples. Furthermore, the m_s of Fe_3O_4 is related to its size [28]. So it can be suggested that the Fe_3O_4 nanoparticles in as-prepared HFC samples are small, which is beneficial to increase the interface between Fe_3O_4 and carbon. In addition, as shown in Table 1, the HFC samples with variable sizes have little change in H_c.

2.3 Microwave absorbing performance

The MA performance of as-prepared samples has been evaluated by the reflection loss (*RL*). The reflection loss (*RL*) is calculated as following:

$$RL = 20\log\left|\frac{Z_{in}-Z_0}{Z_{in}+Z_0}\right| \quad (1)$$

$$Z_{in} = Z_0\sqrt{\frac{\mu_r}{\varepsilon_r}}\tanh\left[j\left(\frac{2\pi}{c}\right)fd\sqrt{\mu_r\varepsilon_r}\right] \quad (2)$$

where Z_{in} is the input characteristic impedance, Z_0 is the impedance of free space, f is the microwave frequency, c is the light velocity, d is the thickness of absorber medium, ε_r ($\varepsilon_r=\varepsilon_r'-j\varepsilon''$) and μ_r ($\mu_r=\mu_r'-j\mu_r''$) are the relative complex permittivity and permeability of absorber medium, respectively.

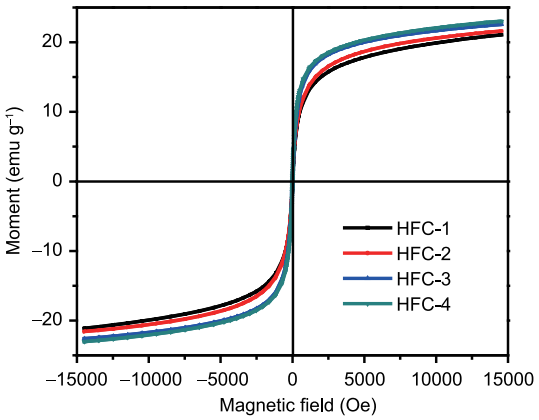

Figure 5 Magnetic hysteresis loops of HFC microspheres (color online).

Table 1 Magnetic parameters of HFC microspheres

Sample	M_s (emu g^{-1})	H_c (Oe)
HFC-1	21.071	11.176
HFC-2	21.616	11.248
HFC-3	22.559	10.834
HFC-4	23.004	10.903

Figure 6 displays the relationship between *RL* and frequency (*f*) of samples with different thickness in the range of 2–18 GHz. At first, comparing the *RL* curves of SFC-2 and HFC-2, it can be easily known that the hollow structure is good for improving the MA performance of absorber, and the resonance frequency (f_{re}) corresponding to the RL_{min} of HFC-2 is higher than that of SFC-2, suggesting that hollow structure makes MA move to the high-frequency region. It may be because that the microwave with high frequency possesses the enough energy to penetrate into the inner of absorber and is absorbed by absorber. Furthermore, contrasting the f_{re} of HFC-*i* samples (i=1,2, 3, 4), it moves to the low frequency with the increasing cavity size, which is to say that there is a negative correlation between cavity size and f_{re}. It has been observed that there is relationship between the MA performance of HFC-*i* (i=1,2, 3, 4) and its inner cavity, and the reflection loss of HFC-3 sample is minimum among them. This indicates that the influence factors on the MA performance have not only cavity size but also the thickness of the spheres shell. When the quality of SiO_2 spheres are certain, the bigger the cavity is, the more the reflecting times of microwave are, and the more the attenuated microwave is. However, the bigger the cavity is, the thinner the spheres shell are, and the less the microwave attenuated by the spheres shell is. Above all, the MA performance of HFC-3 is better than HFC-4.

The thickness of sample (*d*) is also one of the crucial parameters influencing the MA performance of absorber. As shown in Figure 6, the f_{re} of each HFC-*i* sample displays a slight shift to the low frequency with increasing *d*. When *d* is less than 3.0 mm, the RL_{min} of HFC-3 sample is obvious less than that of other HFC-*i* samples, besides its RL_{min} divides into two absorption peaks with further increasing *d*, namely the RL_{min1} corresponding to f_1 and the RL_{min2} corresponding to f_2 ($f_1<f_2$). More interestingly, the absorption bandwidth ($RL<6$) of HFC-3 sample is close to the sum of that of HFC-2 and HFC-4 when *d* is greater than 3.5 mm, which suggests that the HFC-3 sample is the optimal absorber among all HFC samples.

The RL_{min1} of HFC-3 is gradually enhancing with the increasing *d* and may be mainly explained by the quarter-wavelength matching model. According to the quarter-wavelength resonance, the f_{re} at the corresponding thickness *d* can be described by the following equation [29]:

$$f_{re} = \frac{c}{4d\mathrm{Re}(\sqrt{\mu(f)\varepsilon(f)})} \quad (3)$$

With satisfying $f=f_{re}$, where Re() respesents the real number of $\sqrt{\mu(f)\varepsilon(f)}$, $\mu(f)$ and $\varepsilon(f)$ are independently the complex permeability and permittivity at *f*.

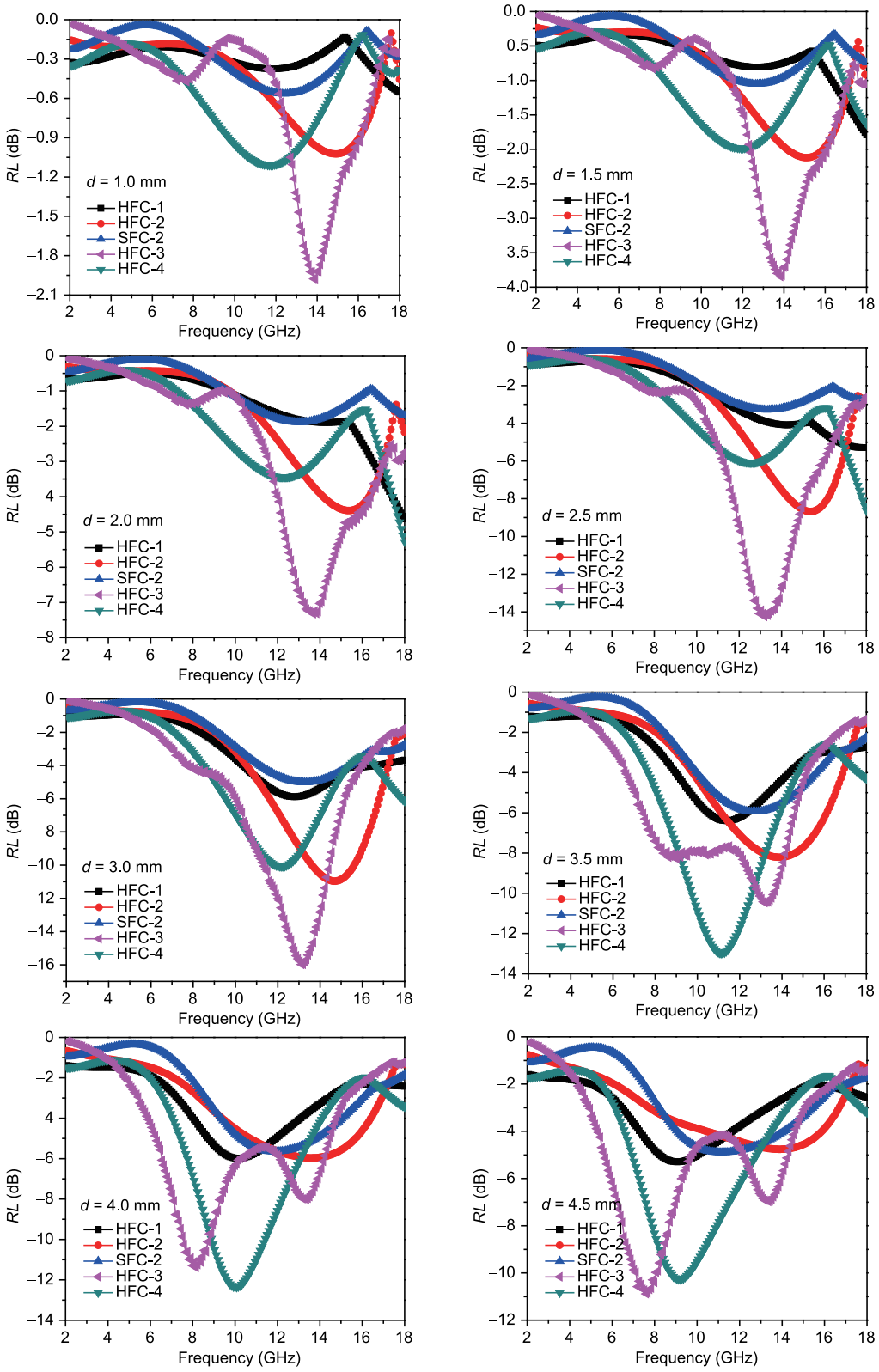

Figure 6 The *RL* curves of samples with different thickness in the frequency range of 2–18 GHz (color online).

Figure 7 shows the simulation results of f_{re} vs. d according to Eq. (3) for HFC-3 sample. It can be seen that the f_1 of HFC-3 sample can well fit the quarter-wavelength model. Notably, the relationship between f and d is in good agreement with the simulation when d is 4.0 mm, showing that the RL_{min1} of HFC-3 can achieve the minimum value at d=4.0 mm, i.e.,

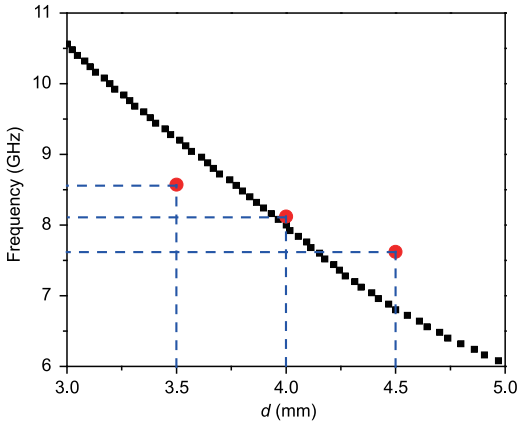

Figure 7 The simulation of f_{re} vs. d under the quarter-wavelength model for HFC-3 sample, where the red dots are the observed values from Figure 6 (color online).

HFC-3 sample has the best MA performance at this thickness, which is in agreement with our experimental results. Therefore, the RL_{min1} of HFC-3 has its root in the quarter-wavelength resonance.

Furthermore, the RL_{min2} of HFC-3 sample may be attributed to its intrinsical magnetic and dielectric loss [30]. The complex permittivity and permeability of HFC-3 sample are displayed in Figure 8(a, b). Notably, the ε' value is obviously larger than ε'', suggesting that HFC-3 sample has the high storage ability of microwave energy. And the complex permittivity is greater than complex permeability, so dielectric loss should make a greater contribution to MA performance of HFC-3 sample. In addition, the dielectric loss tangent ($\tan\delta_e = \varepsilon''/\varepsilon'$) and magnetic loss tangent ($\tan\delta_\mu = \mu''/\mu'$) are applied to evaluate the loss capacity of HFC-3 sample in Figure 8(c). The $\tan\delta_\mu$ and $\tan\delta_\varepsilon$ can obtain the approximate value at about 13.6 GHz, indicating that the HFC-3 sample has the better MA performance in the frequency range of 13–14 GHz due to the good complementarity between magnetic and dielectric loss, which is consistent with the result of Figure 6.

The dielectric loss mainly comes from the conductivity and polarization loss, where the latter includes the dipole orientation and interfacial polarization in the frequency range of 2–18 GHz [31]. According to the free-electron theory, $\varepsilon'' \approx 1/\pi\varepsilon_0\rho f$, where ρ is the resistivity, the low ε'' in Figure 8(a) illuminates a high ρ, which is to say that HFC-3 sample has a poor conductivity. In addition, it is worth noting that the dipolar relaxation of magnetite and carbon can be disregarded in the frequency range of 2–18 GHz [32]. Therefore, the dielectric loss of as-prepared HFC sample mainly comes from interfacial polarization. For the interfacial polarization caused by two media with different conductivity or permittivity, Debye-dipolar relaxation is an important mechanism, which can be validated by the Cole-

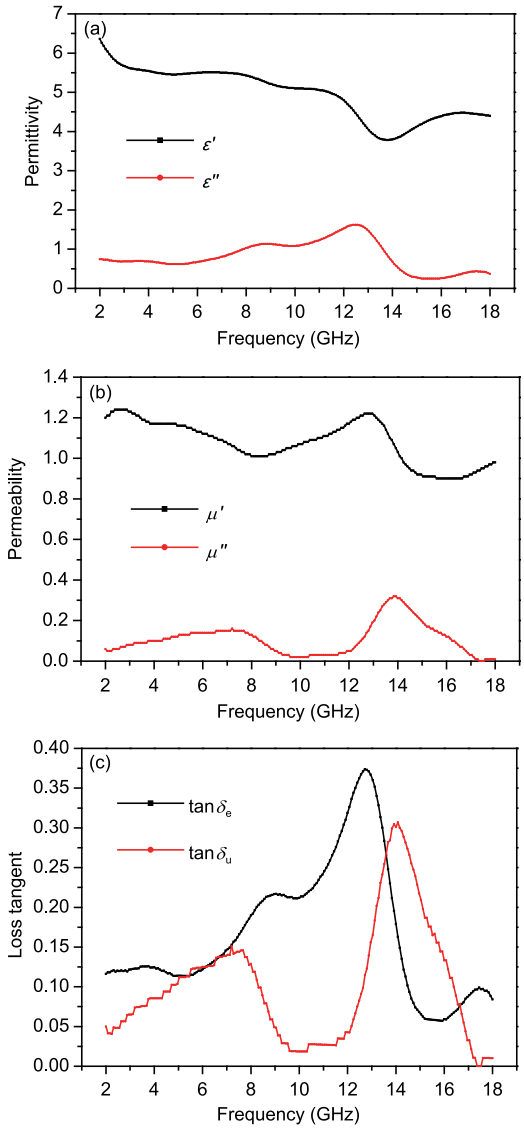

Figure 8 The complex permittivity (a), complex permeability (b), dielectric loss tangent and magnetic loss tangent (c) of HFC-3 sample (color online).

Cole semicircle [33]. The relative complex permittivity ε_r can be described by the following equation:

$$\varepsilon_r = \varepsilon_\infty + \frac{\varepsilon_s - \varepsilon_\infty}{1 + 2j\pi f\tau} = \varepsilon' - j\varepsilon'' \quad (4)$$

where ε_s,ε_∞, f and τ are separately the static permittivity, relative dielectric permittivity at the high-frequency limit, frequency and polarization relaxation time. Thus, ε' and ε'' can be described as follows:

$$\varepsilon' = \varepsilon_\infty + \frac{\varepsilon_s - \varepsilon_\infty}{1 + (2\pi f)^2\tau^2} \quad (5)$$

$$\varepsilon'' = \frac{2\pi f\tau(\varepsilon_s - \varepsilon_\infty)}{1 + (2\pi f)^2\tau^2} \quad (6)$$

Based on Eqs. (5) and (6), the relationship betweem ε' and

ε'' can be obtained:

$$\left(\varepsilon' - \frac{\varepsilon_s + \varepsilon_\infty}{2}\right)^2 + (\varepsilon'')^2 = \left(\frac{\varepsilon_s - \varepsilon_\infty}{2}\right)^2 \quad (7)$$

Therefore, the curve of ε' vs. ε'' is a single semicircle, regarded as the Cole-Cole semicircle.

Figure 9 shows the ε' vs. ε'' curve of HFC-3/paraffin mixture. Two obvious semicircles (I and II) demonstrate that there are two vigorous interfacial polarizations in the HFC-3/paraffin mixture, namely the heterointerface of Fe_3O_4/carbon and Fe_3O_4/paraffin. While the indistinctive semicircle III may be ascribed to the heterointerface of carbon/paraffin due to the similar dielectric constant between carbon and paraffin.

What is more, the MA performance of HFC mixture blended by the equal mass fraction of HFC-2, HFC-3 and HFC-4 is presented in Figure 10, and the evaluation parameters of MA performance obtained from Figure 6 and Figure 10, including the RL_{min}, f_{re} and the best matching thickness of absorber medium (d_{bm}), are presented in Table 2.

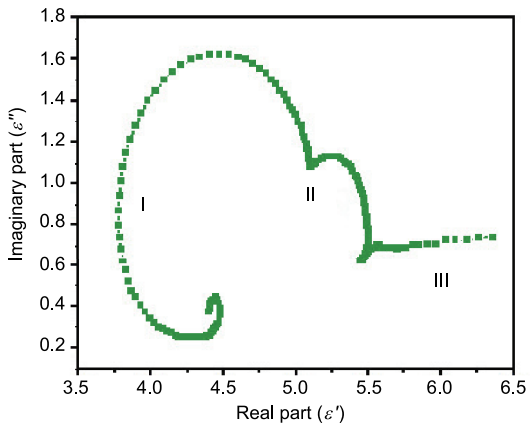

Figure 9 The Cole-Cole semicircle of the HFC-3/paraffin mixture (color online).

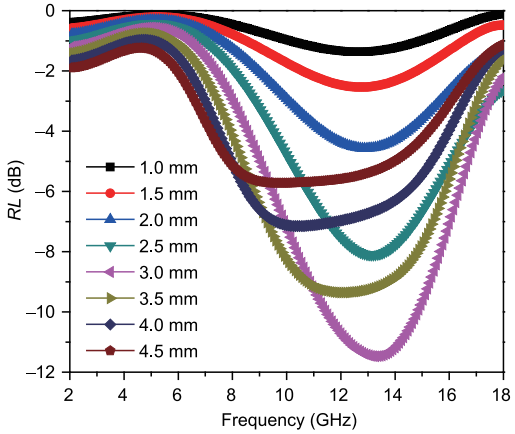

Figure 10 The *RL* curves of HFC mixture with different thickness in the frequency range of 2–18 GHz (color online).

Table 2 The evaluation parameters of MA performance for HFC samples

Sample	RL_{min} (dB)	f_{re} (GHz)	d_{bm} (mm)
HFC-2	−10.9	14.7	3.0
HFC-3	−16.1	13.2	3.0
HFC-4	−13.1	11.1	3.5
HFC mixture	−11.5	13.4	3.0

It can be clearly seen that HFC-3 sample possesses the minimal RL_{min}. As the cavity size increases, f_{re} is reducing and d_{bm} is increasing, suggesting that the cavity size has a great influence on the MA performance. A careful look at the evaluation parameters of HFC mixture reveals that its absorption bandwidth is greater than that of each HFC-*i* sample, and its RL_{min} is the average result of three HFC-*i* samples. So the MA performance of HFC mixture can be reasonably regarded as the comprehensive results of three HFC-*i* samples.

3 Conclusions

In summary, a series of HFC samples have been successfully prepared and displayed different MA performance. By comparing the MA performance of SFC-2 and HFC-2 samples, it can be sure that the hollow structure is good for improving MA performance and can make MA move to the high-frequency region. Furthermore, there is a negative correlation between cavity size and f_{re}. Among all HFC-*i* samples, HFC-3 shows the most excellent MA performance, more interestingly, when d is greater than 3.0 mm, the RL_{min} of HFC-3 divides into two absorption peaks. Its RL_{min1} is gradually enhancing with the increasing d, which can be explained by the quarter-wavelength matching model. In addition, the RL_{min2} of HFC-3 is mainly attributed to its intrinsical magnetic and dielectric loss, in which interfacial polarization makes a great contribution to MA performance. At last, the absorption bandwidth of HFC mixture is greater than that of each HFC-*i* sample, and its RL_{min} is the average result of three HFC-*i* samples. So constructing hollow structure will be a promising route to enhance the MA performance of absorber, and more importantly, the MA performance can be modulated not only by the absorber thickness, but also by the cavity size in absorber to satisfy the application in different frequency bands.

Acknowledgments This work was supported by the National Natural Science Foundation of China (20104017), and the College Students' Science and Technology Innovation Activities Plan of Zhejiang (2014R404056).

Conflict of interest The authors declare that they have no conflict of interest.

Supporting information The supporting information is available online at http://chem.scichina.com and http://link.springer.com/journal/11426. The supporting materials are published as submitted, without typesetting

or editing. The responsibility for scientific accuracy and content remains entirely with the authors.

1 Lv Y, Yu L, Li C, Yang L. *Sci China Chem*, 2016, 59: 142–149
2 Liu Z, Lu G, Yin H, Dang Z, Rittmann B. *Environ Sci Technol*, 2015, 49: 5288–5300
3 Zeng Z, Jin H, Chen M, Li W, Zhou L, Zhang Z. *Adv Funct Mater*, 2016, 26: 303–310
4 Kar GP, Biswas S, Rohini R, Bose S. *J Mater Chem A*, 2015, 3: 7974–7985
5 Liu JW, Xu JJ, Liu ZW, Liu XL, Che RC. *Sci China Chem*, 2014, 57: 3–12
6 Fang J, Liu T, Chen Z, Wang Y, Wei W, Yue X, Jiang Z. *Nanoscale*, 2016, 8: 8899–8909
7 Zhao B, Shao G, Fan B, Wang C, Xie Y, Zhang R. *Powder Technol*, 2015, 270: 20–26
8 Zhu W, Wang L, Zhao R, Ren J, Lu G, Wang Y. *Nanoscale*, 2011, 3: 2862–2864
9 Sözeri H, Mehmedi Z, Kavas H, Baykal A. *Ceram Int*, 2015, 41: 9602–9609
10 Zeng M, Liu J, Yue M, Yang HZ, Dong HR, Tang WK, Jiang H, Liu XF, Yu RH. *J Appl Phys*, 2015, 117: 17B527
11 Shen JH, Chen KY, Li LC, Ding Y, Li JB, Kong WQ. *Sci China Tech Sci*, 2014, 57: 1858–1864
12 Venkatachalam S, Bertin D, Ducournau G, Lampin JF, Hourlier D. *Carbon*, 2016, 100: 158–164
13 Lee SE, Lee WJ, Oh KS, Kim CG. *Carbon*, 2016, 107: 564–572
14 Chen Y, Zhang W, Yang S, Hobiny A, Alsaedi A, Wang X. *Sci China Chem*, 2016, 59: 412–419
15 Shen J, Chen K, Li L, Wang W, Jin Y. *J Alloy Compd*, 2014, 615: 488–495
16 Yu L, Liu Y, Yang F, Evans J, Rodriguez JA, Liu P. *J Phys Chem C*, 2015, 119: 16614–16622
17 Shen J, Feng J, Li L, Tong G, He Y. *J Alloy Compd*, 2015, 632: 490–499
18 Yuan K, Che R, Cao Q, Sun Z, Yue Q, Deng Y. *ACS Appl Mater Interfaces*, 2015, 7: 5312–5319
19 Zhao B, Shao G, Fan B, Zhao W, Xie Y, Zhang R. *J Mater Chem A*, 2015, 3: 10345–10352
20 Li Y, Wu T, Jiang K, Tong G, Jin K, Qian N, Zhao L, Lv T. *J Mater Chem C*, 2016, 4: 7119–7129
21 Panigrahi R, Srivastava SK. *Sci Rep*, 2015, 5: 7638
22 Lv H, Ji G, Liu W, Zhang H, Du Y. *J Mater Chem C*, 2015, 3: 10232–10241
23 Han M, Yin X, Kong L, Li M, Duan W, Zhang L, Cheng L. *J Mater Chem A*, 2014, 2: 16403–16409
24 Zhang Y, Huang Y, Zhang T, Chang H, Xiao P, Chen H, Huang Z, Chen Y. *Adv Mater*, 2015, 27: 2049–2053
25 Moyer JA, Gao R, Schiffer P, Martin LW. *Sci Rep*, 2015, 5: 10363
26 Sun X, He J, Li G, Tang J, Wang T, Guo Y, Xue H. *J Mater Chem C*, 2013, 1: 765–777
27 Shen J, Ma G, Zhang J, Quan W, Li L. *Appl Surface Sci*, 2015, 359: 455–468
28 Sato T, Iijima T, Seki M, Inagaki N. *J Magn Magn Mater*, 1987, 65: 252–256
29 Wen F, Zhang F, Liu Z. *J Phys Chem C*, 2011, 115: 14025–14030
30 Hsiao YC, Wu T, Zang H, Li M, Hu B. *Sci China Chem*, 2015, 58: 239–247
31 Huang Y, Wang Y, Li Z, Yang Z, Shen C, He C. *J Phys Chem C*, 2014, 118: 26027–26032
32 Jazirehpour M, Seyyed Ebrahimi SA. *J Alloy Compd*, 2015, 639: 280–288
33 Zhao B, Zhao W, Shao G, Fan B, Zhang R. *ACS Appl Mater Interfaces*, 2015, 7: 12951–12960